

Low-coverage single-cell mRNA sequencing reveals cellular heterogeneity and activated signaling pathways in developing cerebral cortex

Alex A Pollen^{1,2,4}, Tomasz J Nowakowski^{1,2,4}, Joe Shuga^{3,4}, Xiaohui Wang^{3,4}, Anne A Leyrat³, Jan H Lui^{1,2}, Nianzhen Li³, Lukasz Szpankowski³, Brian Fowler³, Peilin Chen³, Naveen Ramalingam³, Gang Sun³, Myo Thu³, Michael Norris³, Ronald Lebofsky³, Dominique Toppani³, Darnell W Kemp II³, Michael Wong³, Barry Clerkson³, Brittnee N Jones³, Shiquan Wu³, Lawrence Knutsson³, Beatriz Alvarado³, Jing Wang³, Lesley S Weaver³, Andrew P May³, Robert C Jones³, Marc A Unger³, Arnold R Kriegstein^{1,2} & Jay A A West³

Large-scale surveys of single-cell gene expression have the potential to reveal rare cell populations and lineage relationships but require efficient methods for cell capture and mRNA sequencing^{1–4}. Although cellular barcoding strategies allow parallel sequencing of single cells at ultra-low depths⁵, the limitations of shallow sequencing have not been investigated directly. By capturing 301 single cells from 11 populations using microfluidics and analyzing single-cell transcriptomes across downsampled sequencing depths, we demonstrate that shallow single-cell mRNA sequencing (~50,000 reads per cell) is sufficient for unbiased cell-type classification and biomarker identification. In the developing cortex, we identify diverse cell types, including multiple progenitor and neuronal subtypes, and we identify *EGR1* and *FOS* as previously unreported candidate targets of Notch signaling in human but not mouse radial glia. Our strategy establishes an efficient method for unbiased analysis and comparison of cell populations from heterogeneous tissue by microfluidic single-cell capture and low-coverage sequencing of many cells.

To routinely capture single cells, we designed the C₁ Single-Cell Auto Prep System (Fig. 1a). The microfluidic system performs reverse transcription and cDNA amplification in nanoliter reaction volumes (Fig. 1b,c), which increase the effective concentration of reactants and may improve the accuracy of mRNA sequencing (mRNA-seq)⁶. We sequenced libraries from single cells at high coverage (~8.9 × 10⁶ reads per cell) and used the results as a reference to explore the consequences of reduced sequencing depth. To explore the current practical limits of low-coverage sequencing, we pooled dozens of barcoded single-cell libraries in single MiSeq System runs (Illumina; ~2.7 × 10⁵ reads per cell) and downsampled high-coverage results to ultra-low depths. We prepared sequencing libraries after cDNA amplification with the SMARTer Ultra Low RNA Kit for Illumina

Sequencing (Clontech) and the Nextera XT kit (Illumina). Genomic alignment rates and other quality metrics were similar across libraries, whereas empty negative control wells showed no appreciable sequence alignment (<1%) (Supplementary Table 1).

We assessed the accuracy, detection rates and variance of RNA-level estimates from low-coverage sequencing of single-cell libraries by comparing the results with known quantities of spike-in RNA transcripts⁷ and with high-coverage sequencing of the same libraries. The levels of RNA spikes determined by low-coverage mRNA sequencing correlated strongly with the known input quantities ($r = 0.968$; Fig. 1d). For inputs above 32 copies, all spikes could be detected in all samples with minimal variance (Fig. 1e)^{6,8}. In a representative cell, the majority of genes detected by high-coverage sequencing were also detected by low-coverage sequencing (Fig. 1f,g). Of the genes detected by high- but not low-coverage sequencing, the vast majority (98%) were not expressed at high levels (transcripts per million (TPM) > 100), and most (63%) were expressed at low levels (1 < TPM < 10; Supplementary Fig. 1). Across 301 cells from a range of sources, the average correlation between the estimates of single-cell gene expression from low- and high-coverage sequencing was 0.91 (Fig. 1h,i and Supplementary Fig. 2). However, for transcripts with low expression levels (1 < TPM < 10), the correlation dropped to 0.25, demonstrating a limitation in quantifying low-abundance transcripts in individual cells using shallow sequencing. Despite this limitation, combining low-coverage results from as few as ten individual K562 cells accurately reflected results from a pooled population of K562 cells captured by flow cytometry ($r > 0.92$) (Fig. 2a,b). We conclude that single-cell capture and low-coverage sequencing can be used to profile the gene expression of individual cells and that combined results reflect the properties of a given cell population.

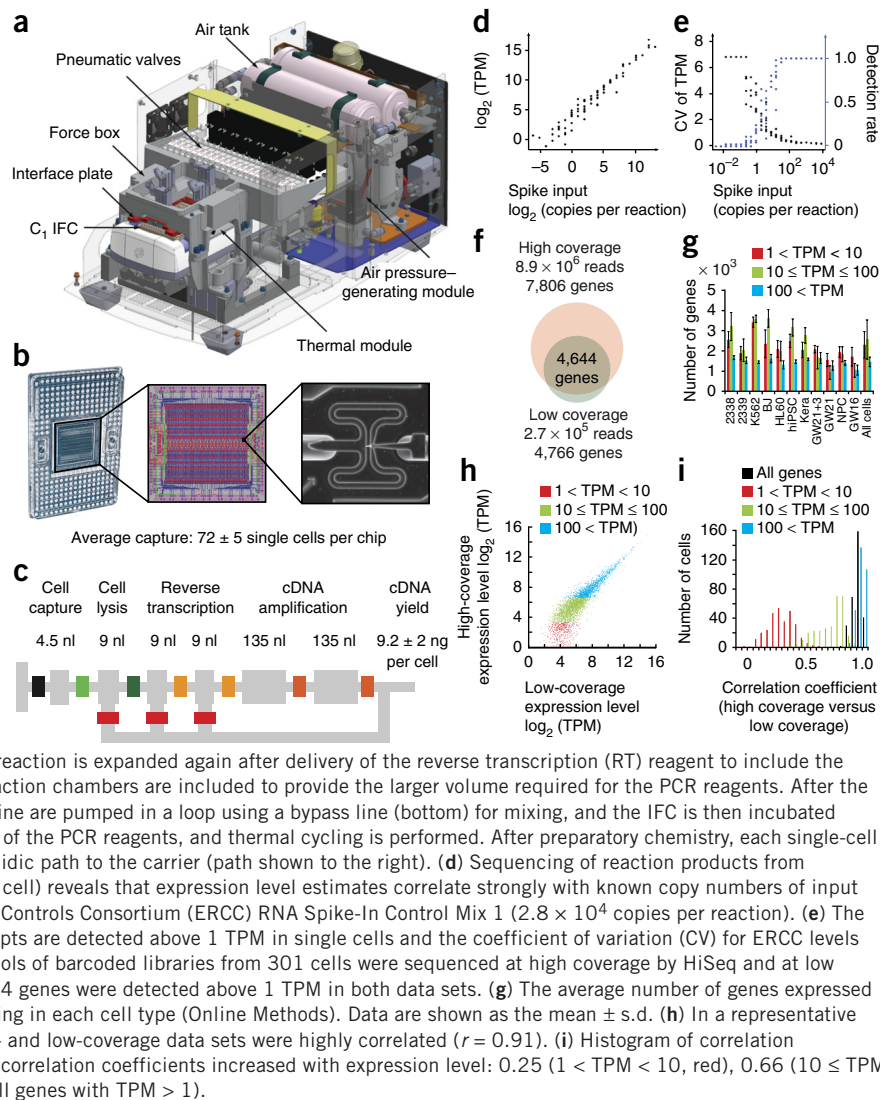
To examine whether low-coverage sequencing can distinguish between cell types, we first compared cells from sources that are expected to show robust differences in gene expression: pluripotent, skin, blood and neural cells (Supplementary Tables 1 and 2).

¹Eli and Edythe Broad Center of Regeneration Medicine and Stem Cell Research, University of California, San Francisco, San Francisco, California, USA. ²Department of Neurology, University of California, San Francisco, San Francisco, California, USA. ³Fluidigm Corporation, South San Francisco, California, USA. ⁴These authors contributed equally to this work. Correspondence should be addressed to A.A.P. (alex.pollen@gmail.com) or A.R.K. (kriegsteina@stemcell.ucsf.edu).

Received 30 January; accepted 25 June; published online 3 August 2014; doi:10.1038/nbt.2967

Figure 1 Capturing single cells and quantifying mRNA levels using the C₁ Single-Cell Auto Prep System. **(a)** Key functional components of the C₁ System are labeled, including the pneumatic components necessary for control of the microfluidic integrated fluidic circuit (IFC) and the thermal components necessary for preparatory chemistry. **(b)** Left, complete IFC with carrier; reagents and cells are loaded into dedicated carrier wells, and reaction products are exported to other dedicated carrier wells. Middle, diagram of the IFC, with connections between the polydimethylsiloxane microfluidic chip and carrier (pink circles), control lines (red), fluidic lines for preparatory chemistry (blue) and lines connecting the control lines (green) shown. Right, a single cell captured in a 4.5-nl capture site; there are 96 captures sites per IFC. The average single-cell capture rate was 72 ± 5 cells (mean \pm s.e.m.) per chip (**Supplementary Tables 1 and 2**). IFC diagram reprinted with permission from ref. 32.

(c) Schematic for a C₁ reaction line, with the reaction line colored light gray and the isolation valves shown in varied colors. All reagents are delivered through a common central bus line (a segment of the bus line is shown on the far left). Each reaction begins in the 4.5-nl capture site. Delivery of the lysis reagent expands the reaction to also include the first 9-nl chamber. The reaction is expanded again after delivery of the reverse transcription (RT) reagent to include the second and third 9-nl chambers. The two 135-nl reaction chambers are included to provide the larger volume required for the PCR reagents. After the addition of RT reagent, the contents of the reaction line are pumped in a loop using a bypass line (bottom) for mixing, and the IFC is then incubated at 42 °C for RT. Mixing is repeated after the addition of the PCR reagents, and thermal cycling is performed. After preparatory chemistry, each single-cell reaction product exits the chip using a dedicated fluidic path to the carrier (path shown to the right). **(d)** Sequencing of reaction products from 46 K562 cells at low coverage (1.7×10^5 reads per cell) reveals that expression level estimates correlate strongly with known copy numbers of input spikes (Pearson's $r = 0.968$) from the External RNA Controls Consortium (ERCC) RNA Spike-In Control Mix 1 (2.8×10^4 copies per reaction). **(e)** The fraction of positive reactions in which ERCC transcripts are detected above 1 TPM in single cells and the coefficient of variation (CV) for ERCC levels are plotted against the spike input amounts. **(f–i)** Pools of barcoded libraries from 301 cells were sequenced at high coverage by HiSeq and at low coverage by MiSeq. **(f)** In a representative cell, 4,644 genes were detected above 1 TPM in both data sets. **(g)** The average number of genes expressed at various levels detected by high-coverage sequencing in each cell type (Online Methods). Data are shown as the mean \pm s.d. **(h)** In a representative cell, the expression levels of genes detected in high- and low-coverage data sets were highly correlated ($r = 0.91$). **(i)** Histogram of correlation coefficients for all single cells ($n = 301$). The mean correlation coefficients increased with expression level: 0.25 ($1 < \text{TPM} < 10$, red), 0.66 ($10 \leq \text{TPM} \leq 100$, green), 0.93 ($\text{TPM} > 100$, blue) and 0.91 (all genes with $\text{TPM} > 1$).

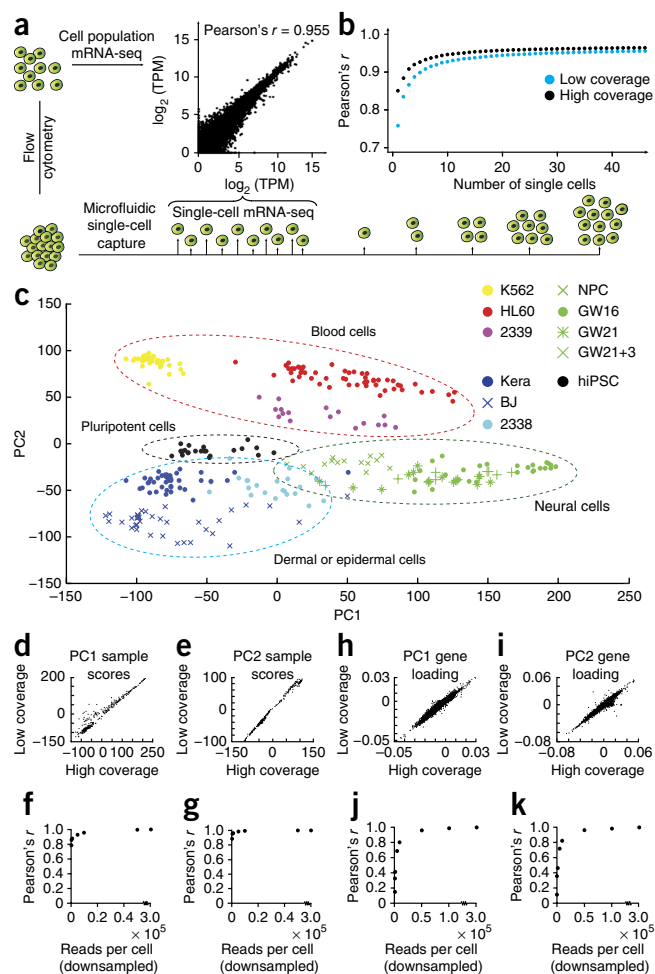


We performed principal component analysis (PCA) of low-coverage sequencing data to identify genes explaining variation across cells. PCA separated the cells into groups corresponding to the source populations (**Fig. 2c** and **Supplementary Figs. 3–5**), and the genes distinguishing each group reflected the biological properties of the cell types (**Supplementary Fig. 5** and **Supplementary Table 3**). PCA of low- and high-coverage sequencing data revealed a remarkably similar graphical distribution of analyzed cells, and the majority (78%) of the top 500 genes determined by PCA were shared between PCA performed on low- and high-coverage data (**Supplementary Figs. 4 and 6** and **Supplementary Table 4**). We next examined the minimal depth at which low-coverage sequencing could be applied to describe variation across diverse cell types. The positions of cells along PC1 and PC2 were highly correlated between the low- and high-coverage sequencing results (**Fig. 2d,e**) and could be accurately predicted by sequencing cells at ultra-low depths of less than 10,000 reads per cell (**Fig. 2f,g** and **Supplementary Fig. 4**). Similarly, low-coverage sequencing provided accurate estimates of the contribution of genes to the loading of PC1 and PC2 (**Fig. 2h,i**) but required at least 50,000 reads per cell (**Fig. 2j,k**). Thus, even at ultra-low depths where the levels of individual genes are difficult to estimate, the combination of the abundant genes that vary across cells permits classification of cells.

To explore whether low-coverage single-cell mRNA-seq is sufficient to distinguish closely related cell types from heterogeneous populations, we further analyzed single cells derived from the developing human cortex during phases of neurogenesis. Excitatory neurons of the cerebral cortex are born from radial glia, which reside in the germinal zones of the dorsal telencephalon: the ventricular and sub-ventricular zones⁹. Before reaching their terminal positions in the cortical plate, newborn neurons migrate through the germinal and intermediate zones. Defects in the specification and migration of newborn neurons underlie the pathogenesis of many neurodevelopmental disorders¹⁰, but studying these transient populations of cells in heterogeneous tissue has been challenging. We collected single cells from the germinal zone of human cortex at gestational week (GW) 16, aiming to capture radial glia and newly generated cortical neurons. To analyze cell diversity in the context of neural differentiation, we also collected primary cells from the cortex at GW21 and further cultured a subset of these cells for 3 weeks (GW21+3). Similarly, to represent more immature neuroepithelial cells, we collected neural progenitors derived from pluripotent stem cells (**Fig. 3a**).

We analyzed variation across cells derived from these four neural sources using PCA (**Supplementary Figs. 7 and 8**). Hierarchical clustering of cells on the basis of the 500 genes explaining the most

Figure 2 Low-coverage single-cell mRNA sequencing is sufficient to detect genes contributing to cell identity. (a) Average expression levels from single-cell mRNA sequencing of 46 K562 cells correlate strongly with expression levels from a population of 100 K562 cells isolated by flow cytometry. (b) The correlation between individual K562 cells and the population improves with diminishing returns as additional single-cell results are combined. (c) Distinct groups of cells corresponding to pluripotent, blood, skin and neural cells can be identified by PCA of 301 cells sequenced at low coverage. NPC, neural progenitor cell. (d–g) Sample scores from low- and high-coverage data were calculated using the eigenvectors from high-coverage data and correlate strongly across all 301 cells for PC1 (d, $r = 0.973$) and PC2 (e, $r = 0.997$). The strong sample score correlations ($r > 0.92$) persist with as few as 5,000 reads per cell for PC1 (f) and PC2 (g). (h–k) Similarly, eigenvectors derived from the low- and high-coverage data sets correlate strongly for the eigenvectors defining PC1 (h, $r = 0.980$) and PC2 (i, $r = 0.956$), but strong correlations of eigenvectors ($r > 0.95$) for PC1 (j) and PC2 (k) require at least 50,000 reads per cell.



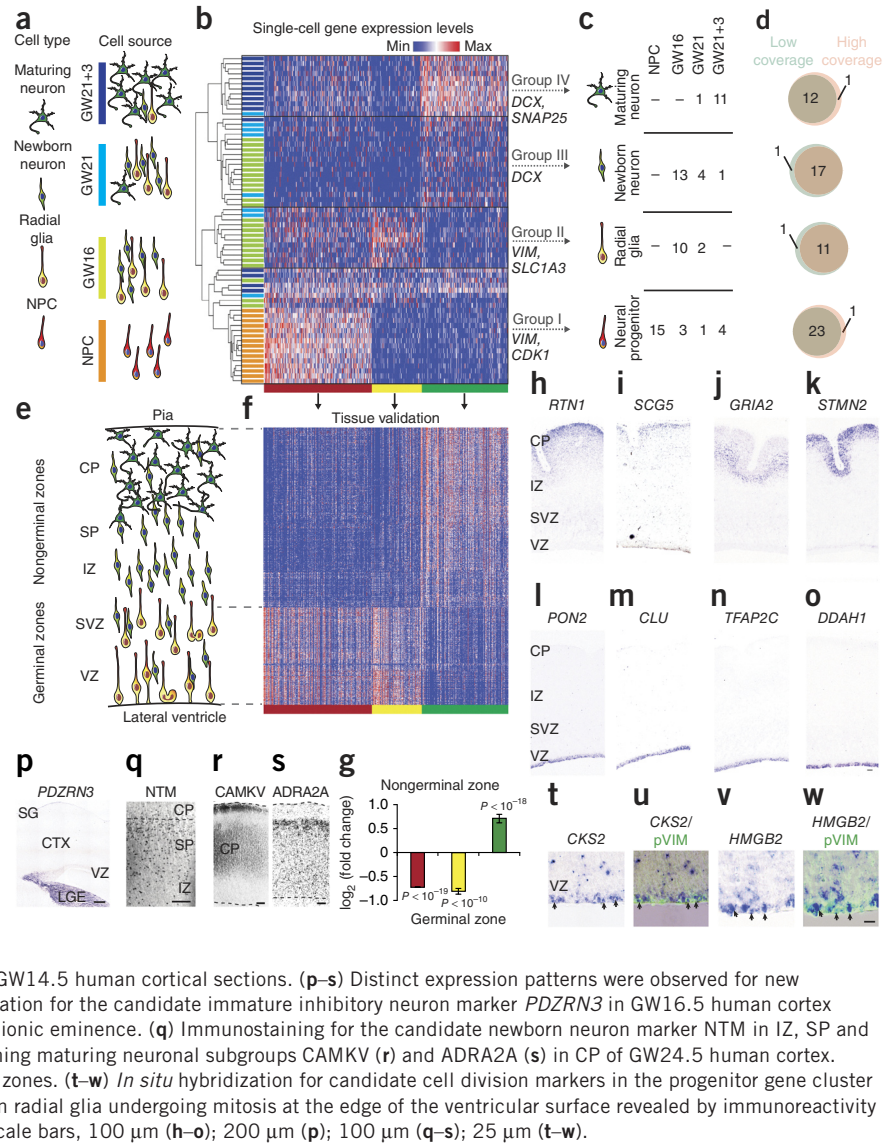
variation in PC1, PC2 and PC3 separated the cells into four broad groups, with cells from each source contributing to multiple groups (Fig. 3b,c). The group membership of individual cells largely overlapped between the high- and low-coverage sequencing data (Fig. 3d) and could be identified at downsampled depths of between 5,000 and 50,000 reads per cell (Supplementary Figs. 9 and 10). Cells in groups I and II expressed high levels of neuroepithelial markers, including *VIM*, *SOX2* and *PAX6*. In addition, cells in group I also expressed high levels of the proliferative markers *CDK1* and *ASPM*, whereas cells in group II expressed high levels of the mature radial glial markers *SLC1A3* and *HES1*. In contrast, cells in groups III and IV expressed the pan-neuronal marker *DCX*, and cells in group IV also expressed many markers of neuronal maturation, including *MEF2C*, *SATB2* and *SNAP25* (Supplementary Figs. 10 and 11). Thus, we interpreted the groups to represent dividing neural progenitors (group I), radial glia (group II), newborn neurons (group III) and maturing neurons (group IV). To independently validate our results, we examined the expression of genes distinguishing each group across 599 tissue samples collected from distinct regions of the developing human cortex¹¹. Genes defining neural progenitors and radial glia in the single-cell analysis were strongly enriched in germinal zones, whereas genes defining newborn and maturing neurons were strongly enriched outside of germinal zones (Fig. 3e–g and Supplementary Table 5). Similarly, *in situ* hybridization confirmed that newly identified markers of radial glia, newborn and maturing neurons are expressed in zones where these cell types are abundant (Fig. 3h–o and Supplementary Figs. 12 and 13).

In addition to the four broad groups identified using hierarchical clustering, distinct subgroups also corresponded to other known and potentially new cell types (Supplementary Figs. 10 and 11). For example, cells in group Ib expressed multiple markers of intermediate neural progenitors³. Cells in group IIIb expressed the canonical markers of inhibitory interneurons *GAD1* and *DLX* genes, as well as previously unreported markers such as *PDZRN3* (Fig. 3p), whereas the remaining cells in group III expressed the proneural genes *NEUROD1* and *NEUROD6*. In addition, group III cells expressed *UNC5D*, a gene that is transiently upregulated in newly generated mouse excitatory neurons and is required for the earliest phases of migration¹², and other genes such as *ROBO2* and *NTM* (Fig. 3q), whose possible roles in newborn cortical neurons remain to be investigated. Group IV could be further divided into maturing neurons expressing high levels of *CAMKV* and cells expressing high levels of *ADRA2A* (Supplementary Fig. 11). Complementary expression patterns of *CAMKV* and *ADRA2A* proteins in the cortical plate (Fig. 3r,s) indicate that these

finer subgroups may reflect additional heterogeneity within maturing cortical neurons. Although many of the genes explaining variation across single cells related to cell identity, a subset of genes with strong PCA loading were enriched for mitotic markers and have not been studied in radial glia development (Supplementary Fig. 13). The candidate mitotic markers *CKS2* and *HMGB2* were detected specifically in a subset of human radial glia undergoing cell division at the edge of the lateral ventricle (Fig. 3t–w). Thus, low-coverage sequencing of single cells collected from primary tissue can be used to identify cell types, states and candidate biomarkers.

Transcription of immediate early genes has been studied extensively in activated neurons^{13–15}, but the strong PCA loading scores of *EGR1* and *FOS* suggest that their expression may also reflect important aspects of cellular diversity in the developing cortex (Supplementary Fig. 13 and Supplementary Table 5). Indeed, *in situ* hybridization revealed mosaic expression of *EGR1* and *FOS* in the ventricular zone (Fig. 4a–d). The levels of *EGR1* and *FOS* were highly correlated across single radial glial cells, and the corresponding proteins were coexpressed in a subset of radial glia, suggesting that these genes could be transcribed in response to the same signaling pathway (Fig. 4e,h and Supplementary Fig. 14). Multiple signaling pathways, including FGF, Notch and Wnt, orchestrate radial glia development, but asynchronous activation of these signaling pathways in neighboring cells makes identifying downstream effector genes challenging^{16,17}. Coordinated patterns of pathway activation in other tissues have facilitated the identification of candidate downstream effector genes,

Figure 3 Low-coverage single-cell mRNA sequencing distinguishes diverse neural cell types and identifies biomarkers in heterogeneous tissue. **(a)** Schematic of cell types and sources selected to represent stages of neuronal differentiation. Cultured neural progenitor cells (NPC) represent early undifferentiated stages, and primary cortical samples are expected to contain radial glia, as well as newborn and maturing neurons. **(b)** Hierarchical clustering of 65 single cells across 500 genes with the strongest PC1–PC3 loading scores identifies four major groups of cells (I–IV), and *k*-means clustering identifies three clusters of genes (red, yellow and green). **(c)** Major groups can be interpreted on the basis of the expression of known genes. The table shows the number of cells of specific types captured from each source. **(d)** Cell classification on the basis of low-coverage data largely overlaps with classification based on high-coverage data. **(e)** Schematic of the distribution of cell types in the developing cortex at midgestation. VZ, ventricular zone; SVZ, subventricular zone; IZ, intermediate zone; SP, subplate; CP, cortical plate. **(f)** Heat map of gene expression values for PCA genes (columns) in 599 regions of the developing cortex¹¹ (rows). **(g)** Genes belonging to the red cluster ($n = 218$) and yellow cluster ($n = 98$) are enriched in VZ and SVZ, whereas genes belonging to the green cluster ($n = 176$) are enriched in IZ, SP and CP; *P* values were calculated using Wilcoxon signed-rank test. Error bars, s.d. **(h–o)** *In situ* hybridization for representative genes belonging to the neuronal (green) cluster, including *RTN1* (**h**), *SCG5* (**i**), *GRIA2* (**j**) and *STMN2* (**k**), and genes belonging to the radial glia (yellow) cluster, including *PON2* (**l**), *CLU* (**m**), *TFAP2C* (**n**) and *DDAH1* (**o**), in GW14.5 human cortical sections. **(p–s)** Distinct expression patterns were observed for new candidate markers of subgroups. **(p)** *In situ* hybridization for the candidate immature inhibitory neuron marker *PDZRN3* in GW16.5 human cortex (CTX). SG, subplate granular layer; LGE, lateral ganglionic eminence. **(q)** Immunostaining for the candidate newborn neuron marker NTM in IZ, SP and CP. **(r,s)** Immunostaining for the markers distinguishing maturing neuronal subgroups CAMKV (**r**) and ADRA2A (**s**) in CP of GW24.5 human cortex. The dashed lines in **q–s** highlight the borders of the zones. **(t–w)** *In situ* hybridization for candidate cell division markers in the progenitor gene cluster (red) showing *CKS2* (**t**) and *HMGB2* (**v**) expression in radial glia undergoing mitosis at the edge of the ventricular surface revealed by immunoreactivity for phosphorylated (Ser82) vimentin (pVIM; **u,w**). Scale bars, 100 μ m (**h–o**); 200 μ m (**p**); 100 μ m (**q–s**); 25 μ m (**t–w**).



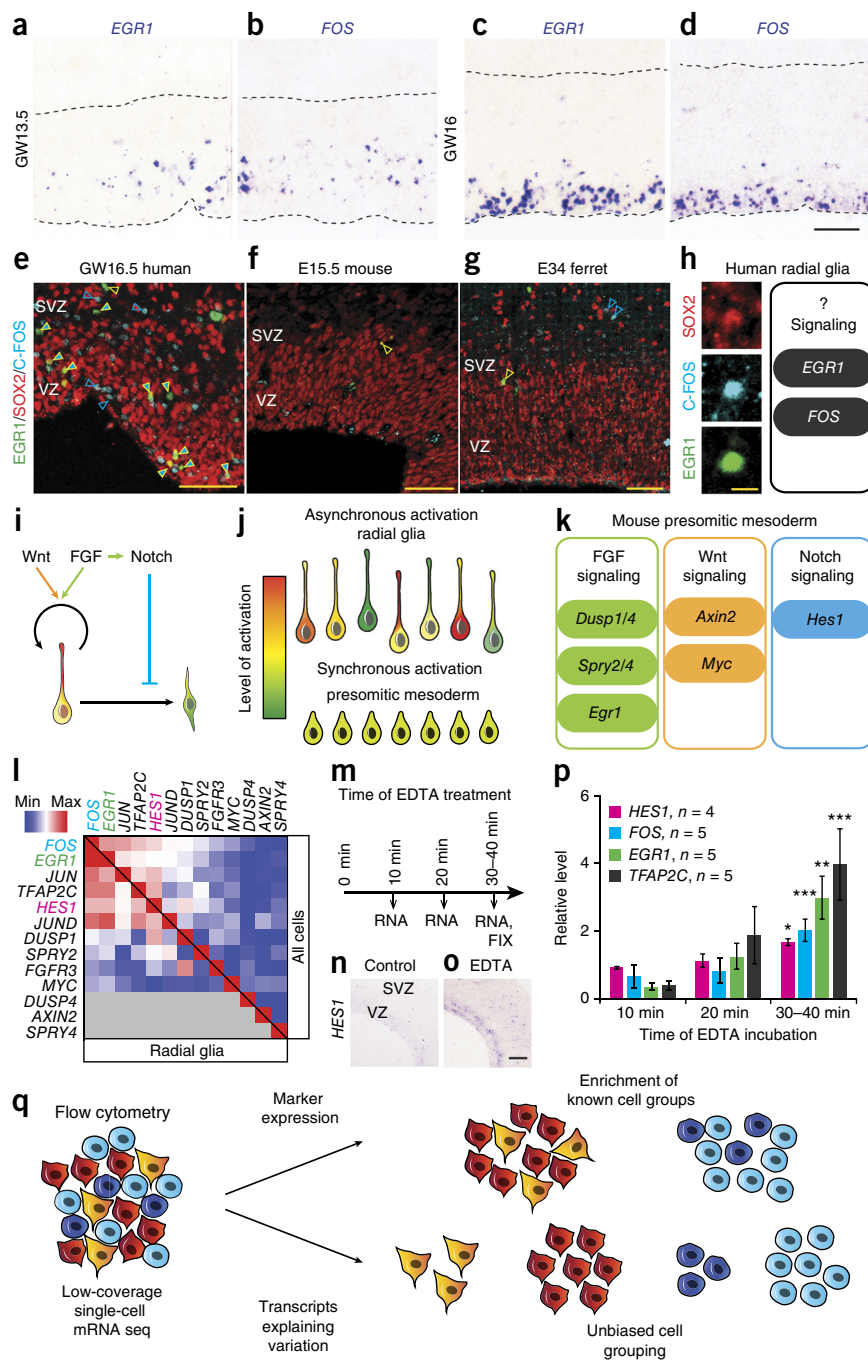
but these target genes often depend on cellular context and vary across species^{16,18} (Fig. 4i–k).

To determine which signaling pathway might be responsible for the coordinated activation of immediate early genes in human radial glia, we examined the correlation of *EGR1* and *FOS* mRNA levels with the levels of canonical signaling pathway effector genes that have been established by studies of other developmental processes. Across single cells, *EGR1* and *FOS* mRNA correlated more strongly with the Notch effector *HES1* than with the FGF effectors *DUSP1*, *DUSP4*, *SPRY2* or *SPRY4* or the WNT effectors *AXIN2* or *MYC* (Fig. 4l and Supplementary Fig. 15). To examine whether activation of Notch signaling induces changes in *EGR1* and *FOS* expression, we activated Notch signaling in cultured human cortical slices by removing extracellular calcium¹⁹. Incubation of primary human cortical slices with EDTA induced a rapid (30–40 min) increase in the levels of *HES1*, as well as *EGR1*, *FOS* and another highly correlated gene, *TFAP2C* (Fig. 4m–p). In other stem cell contexts, *EGR1* and *FOS* have a role in quiescence and retention in the stem cell niche^{20–22}, but the role of these genes as candidate Notch targets in radial glia remains to be examined. Notably, *EGR1* and C-FOS were rarely detected in mouse

or ferret radial glia (Fig. 4e–g and Supplementary Fig. 14), indicating that these factors could contribute to differences in radial glia development across species, which include a markedly longer G1 phase and increased proliferative capacity in human radial glia²³. Together our findings suggest that low-coverage single-cell analysis can be more generally applied to identify cells in different states of signaling pathway activation and candidate downstream target genes.

Identifying gene expression profiles of cells of the same type or state has numerous applications in modern biology. Here we demonstrate that ultra-low coverage sequencing of single cells (<10,000 reads) is sufficient for unbiased classification of diverse cell types in heterogeneous tissue but that finer distinctions within categories and resolution of the set of genes explaining variation require moderately higher depths (~50,000 reads). Increased sequencing coverage beyond these depths likely provides diminishing returns because single cells contain a limited number of transcripts (~300,000), and the amplification steps used to generate sequencing libraries sample a subset (~40%) of the transcriptome^{24–26}. Using our shallow sequencing strategy, we identified numerous cell type-specific biomarkers across a range of cell types in the midgestation human

Figure 4 EGR1 and FOS are candidate targets of Notch signaling in human radial glia identified using low-coverage single-cell mRNA-seq. (a,b) *In situ* hybridization images of human VZ at GW13.5 showing cells sparsely labeled for EGR1 (a) and FOS (b). (c,d) At GW16, pronounced mosaic expression of EGR1 (c) and FOS (d) was detected in the apical portion of VZ. Dashed lines indicate the apical and basal edges of the VZ. Scale bar, 50 μ m (a–d). (e–g) EGR1 and FOS proteins are detected in a subset of SOX2-expressing cells in the human ventricular zone (e) but rarely colabel with SOX2-expressing cells in mouse (f) or ferret (g) at similar developmental stages. E, embryonic day. Filled arrows, triple-labeled cells; yellow arrows, EGR1- and SOX2-expressing cells; blue arrows, C-FOS- and SOX2-expressing cells; scale bars, 50 μ m. (h) High-magnification example of a SOX2-expressing (red) cell in human VZ that is immunoreactive for C-FOS (cyan) and EGR1 (green); scale bar, 10 μ m. The schematic represents the hypothesis that expression of EGR1 and FOS *in vivo* in human radial glia could be elicited in response to activated signaling pathways. (i) Schematic showing the key developmental signaling pathways regulating radial glia development. (j) Asynchronous activation of signaling pathways makes the identification of downstream target genes challenging in heterogeneous tissue. (k) Schematic showing the key candidate effector genes of FGF, Wnt and Notch signaling in mouse presomitic mesoderm. *Dusp1/4*, *Dusp1* and *Dusp4*; *Spry2/4*, *Spry2* and *Spry4*. (l) Heat map showing correlation coefficients between mRNA levels for EGR1, FOS, other immediate early genes and canonical effectors of FGF, Notch and Wnt signaling pathway across all 65 neural cells (above the diagonal) and within radial glia (below the diagonal). (m) Schematic showing the experimental design for stimulating Notch signaling in organotypic slice cultures of human cortex using EDTA. (n,o) *In situ* hybridization for HES1 in control (n) and experimental (o) slices. Scale bar, 50 μ m (n,o). (p) Quantification of mRNA levels of HES1, FOS, EGR1 and TFAP2C ($n = 4$ –5 independent samples, 2–3 slices per condition). All quantitative RT-PCR results represent the average \pm s.e.m. calculated using the $-\Delta\Delta C_t$ method, and P values were calculated using paired two-tailed Student's t -test. * $P < 0.05$, ** $P < 0.01$, *** $P < 0.001$. (q) Low-coverage mRNA-seq of single cells permits *in silico* sorting of cells on the basis of cell type or state. Flow cytometry uses established staining characteristics to enrich for known cell types in heterogeneous samples. In contrast, low-coverage single-cell mRNA-seq identifies the major genes explaining variation across single cells, allowing for unbiased discovery and further analysis of distinct cell populations and states.



cortex, including radial glia in different stages of cell cycle progression and signaling pathway activation, and newly generated neurons in the earliest phases of migration. Few specific markers exist for the purification of these distinct cell states and transient developmental intermediates using flow cytometry. In contrast to flow cytometry, low-coverage single-cell sequencing detects thousands of abundant transcripts that can be analyzed to group cells according to cell type or state (Fig. 4q). Although the observed level of a given transcript in a single cell can vary because of transcriptional bursts and technical noise associated with low quantities of input RNA^{8,27,28},

the simultaneous profiling of multiple differentially expressed transcripts enables unbiased discovery of cell groups on the basis of shared signatures of gene expression^{29–31}. By grouping cells of a given identity, the bulk transcriptome for that population may then be accurately reconstructed⁶. We anticipate that the unbiased classification of cells by efficient low-coverage single-cell sequencing will be applied to large-scale surveys of primary tissue samples to identify cell type-specific biomarkers, compare gene expression in cells of a given type across samples and reconstruct developmental lineages of related cell types.

METHODS

Methods and any associated references are available in the [online version of the paper](#).

Accession codes. Relevant data sets, including raw reads, have been deposited in the NCBI Sequence Read Archive (<http://www.ncbi.nlm.nih.gov/Traces/sra/>) under accession number [SRP041736](#).

Note: Any Supplementary Information and Source Data files are available in the online version of the paper.

ACKNOWLEDGMENTS

We thank M. Bershteyn (University of California, San Francisco (UCSF)), E. Di Lullo (UCSF), C. Gertz (UCSF), C. McLean (23andMe), F. Ng (Fluidigm Corporation), J. Liu (UCSF), C. Lowe (Stanford University), M. Oldham (UCSF), A. Diaz (UCSF) and H. Retallack (UCSF) for reading the manuscript and for useful suggestions, S. Wang and Y. Wang for technical assistance, K. Davies (University of Oxford) for providing the antibody to syncoilin, A. Simeone (Institute of Genetics and Biophysics, Adriano Buzzati-Traverso) for providing the *Emx2* probe, S. Yao and S. Ku (Allen Institute for Brain Research) for assistance in the neural progenitor induction protocol, G. Wang (Stanford University) for providing human induced pluripotent stem cells (hiPSCs) and the staff at the San Francisco General Hospital for providing access to donated fetal tissue. L.S., N.L. and M.A.U. are partially supported by California Institute for Regenerative Medicine Tools and Technologies II grant RT2-02052 to M.A.U., and the generation and maintenance of the hiPSCs and neural progenitor cells was also supported by RT2-02052 to M.A.U. A.A.P. is supported by a Damon Runyon Cancer Research Foundation postdoctoral fellowship (DRG-2166-13). This research was also supported by National Institute of Neurological Disorders and Stroke awards R01NS075998 and R01NS072630 to A.R.K.

AUTHOR CONTRIBUTIONS

A.A.P., A.A.L., J.A.A.W., J.S., T.J.N. and X.W. conceived and designed the study. A.A.P., A.A.L., B.A., J.H.L., J.S., J.W., L.K., L.S., N.L., P.C. and T.J.N. performed experiments. A.A.P., A.A.L., J.S., S.W., T.J.N. and X.W. analyzed the data. A.A.L., A.P.M., B.C., B.F., B.N.J., D.W.K., D.T., G.S., J.S., J.A.A.W., J.W., M.T., M.N., M.W., N.R., P.C., R.L., L.S.W. and X.W. were involved in system development. A.P.M., A.R.K., J.A.A.W., M.A.U. and R.C.J. supervised the project, helped with design and interpretation, and provided laboratory space and financial support. A.A.P., J.S. and T.J.N. wrote the manuscript with input from all authors.

COMPETING FINANCIAL INTERESTS

The authors declare competing financial interests: details are available in the [online version of the paper](#).

Reprints and permissions information is available online at <http://www.nature.com/reprints/index.html>.

- Shalek, A.K. *et al.* Single-cell transcriptomics reveals bimodality in expression and splicing in immune cells. *Nature* **498**, 236–240 (2013).
- Shapiro, E., Biezuner, T. & Linnarsson, S. Single-cell sequencing-based technologies will revolutionize whole-organism science. *Nat. Rev. Genet.* **14**, 618–630 (2013).
- Kawaguchi, A. *et al.* Single-cell gene profiling defines differential progenitor subclasses in mammalian neurogenesis. *Development* **135**, 3113–3124 (2008).
- Treutlein, B. *et al.* Reconstructing lineage hierarchies of the distal lung epithelium using single-cell RNA-seq. *Nature* **509**, 371–375 (2014).
- Jaitin, D.A. *et al.* Massively parallel single-cell RNA-seq for marker-free decomposition of tissues into cell types. *Science* **343**, 776–779 (2014).

- Wu, A.R. *et al.* Quantitative assessment of single-cell RNA-sequencing methods. *Nat. Methods* **11**, 41–46 (2014).
- Jiang, L. *et al.* Synthetic spike-in standards for RNA-seq experiments. *Genome Res.* **21**, 1543–1551 (2011).
- Brennecke, P. *et al.* Accounting for technical noise in single-cell RNA-seq experiments. *Nat. Methods* **10**, 1093–1095 (2013).
- Kriegstein, A., Noctor, S. & Martinez-Cerdeno, V. Patterns of neural stem and progenitor cell division may underlie evolutionary cortical expansion. *Nat. Rev. Neurosci.* **7**, 883–890 (2006).
- Ross, M.E. & Walsh, C.A. Human brain malformations and their lessons for neuronal migration. *Annu. Rev. Neurosci.* **24**, 1041–1070 (2001).
- Miller, J.A. *et al.* Transcriptional landscape of the prenatal human brain. *Nature* **508**, 199–206 (2014).
- Miyoshi, G. & Fishell, G. Dynamic FoxG1 expression coordinates the integration of multipolar pyramidal neuron precursors into the cortical plate. *Neuron* **74**, 1045–1058 (2012).
- Tarcic, G. *et al.* EGR1 and the ERK-ERF axis drive mammary cell migration in response to EGF. *FASEB J.* **26**, 1582–1592 (2012).
- Bièche, I. *et al.* Molecular profiling of inflammatory breast cancer: identification of a poor-prognosis gene expression signature. *Clin. Cancer Res.* **10**, 6789–6795 (2004).
- Fischer, A.J., Scott, M.A., Ritchey, E.R. & Sherwood, P. Mitogen-activated protein kinase-signaling regulates the ability of Muller glia to proliferate and protect retinal neurons against excitotoxicity. *Glia* **57**, 1538–1552 (2009).
- Krol, A.J. *et al.* Evolutionary plasticity of segmentation clock networks. *Development* **138**, 2783–2792 (2011).
- Shimojo, H., Ohtsuka, T. & Kageyama, R. Oscillations in notch signaling regulate maintenance of neural progenitors. *Neuron* **58**, 52–64 (2008).
- Hansson, M.L. *et al.* MAML1 acts cooperatively with EGR1 to activate EGR1-regulated promoters: implications for nephrogenesis and the development of renal cancer. *PLoS ONE* **7**, e46001 (2012).
- Housden, B.E. *et al.* Transcriptional dynamics elicited by a short pulse of notch activation involves feed-forward regulation by E(spl)/Hes genes. *PLoS Genet.* **9**, e1003162 (2013).
- Min, I.M. *et al.* The transcription factor EGR1 controls both the proliferation and localization of hematopoietic stem cells. *Cell Stem Cell* **2**, 380–391 (2008).
- Okada, S., Fukuda, T., Inada, K. & Tokuhisa, T. Prolonged expression of c-fos suppresses cell cycle entry of dormant hematopoietic stem cells. *Blood* **93**, 816–825 (1999).
- Bonnert, T.P. *et al.* Molecular characterization of adult mouse subventricular zone progenitor cells during the onset of differentiation. *Eur. J. Neurosci.* **24**, 661–675 (2006).
- Kornack, D.R. & Rakic, P. Changes in cell-cycle kinetics during the development and evolution of primate neocortex. *Proc. Natl. Acad. Sci. USA* **95**, 1242–1246 (1998).
- Islam, S. *et al.* Characterization of the single-cell transcriptional landscape by highly multiplex RNA-seq. *Genome Res.* **21**, 1160–1167 (2011).
- Deng, Q., Ramsköld, D., Reinius, B. & Sandberg, R. Single-cell RNA-seq reveals dynamic, random monoallelic gene expression in mammalian cells. *Science* **343**, 193–196 (2014).
- Sims, D., Sudbery, I., Ilott, N.E., Heger, A. & Ponting, C.P. Sequencing depth and coverage: key considerations in genomic analyses. *Nat. Rev. Genet.* **15**, 121–132 (2014).
- Faddah, D.A. *et al.* Single-cell analysis reveals that expression of nanog is biallelic and equally variable as that of other pluripotency factors in mouse ESCs. *Cell Stem Cell* **13**, 23–29 (2013).
- Islam, S. *et al.* Quantitative single-cell RNA-seq with unique molecular identifiers. *Nat. Methods* **11**, 163–166 (2014).
- Dalerba, P. *et al.* Single-cell dissection of transcriptional heterogeneity in human colon tumors. *Nat. Biotechnol.* **29**, 1120–1127 (2011).
- Ramsköld, D. *et al.* Full-length mRNA-Seq from single-cell levels of RNA and individual circulating tumor cells. *Nat. Biotechnol.* **30**, 777–782 (2012).
- Guo, G. *et al.* Resolution of cell fate decisions revealed by single-cell gene expression analysis from zygote to blastocyst. *Dev. Cell* **18**, 675–685 (2010).
- Shalek, A.K. *et al.* Single-cell RNA-seq reveals dynamic paracrine control of cellular variation. *Nature* **509**, 363–369 (2014).

ONLINE METHODS

Origin of cell lines and tissue samples. hiPSCs were originally derived from neonatal male human foreskin BJ fibroblasts by G. Wang at the Department of Genetics at Stanford University using Sendai virus from Life Technologies (A16517). Cultured undifferentiated hiPSCs were maintained in Essential 8 Medium (Life Technologies). StainAlive Tra-1-60 antibody (DyLight 488) staining (Stemgent) was used to confirm an undifferentiated state. After a dissociation with StemPro Accutase Cell Dissociation Reagent (Life Technologies), single cells were plated onto Matrigel-coated plates at 2.5×10^5 cells per cm^2 . NPC differentiation was induced using DMEM and F-12 medium (GIBCO DMEM and Nutrient Mixture F-12 from Life Technologies) supplemented with B27 (without vitamin A; Life Technologies, 12587010), N-2 (Life Technologies), 0.1 mM nonessential amino acids (Sigma), 0.5% bovine serum albumin (Sigma), 1 mM β -mercaptoethanol (BME; Sigma), 50 nM LDN-193189 (Stemgent), 5 μM SB431542 (Stemgent) and 1 μM Stemolecule Cyclopamine (Stemgent). After 12 d in culture, >90% of cells were immunopositive for PAX6.

ATCC PCS-200-010 cell (foreskin keratinocytes, abbreviated Kera) culture was maintained in the dermal cell basal medium ATCC PCS-200-030 supplemented with the keratinocyte growth kit (ATCC PCS-200-040). ATCC CRL-2338 cells (derived from a primary stage IIA, grade 3 invasive ductal carcinoma with no lymph node metastases, abbreviated CRL-2338) were cultured in the complete growth medium RPMI-1640 (ATCC 30-2001) supplemented with 10% fetal bovine serum (FBS; GIBCO 16000-077). ATCC CRL-2339 cells (Epstein-Barr virus-transformed B lymphoblasts, abbreviated CRL-2339) were cultured in the growth medium RPMI-1640 (ATCC 30-2001) supplemented with 10% FBS. ATCC CCL-240 cells (promyeloblastic peripheral blood leukocytes obtained by leukopheresis from a patient with acute promyelocytic leukemia, abbreviated HL60) were cultured in Iscove's modified Dulbecco's medium (IMDM) (ATCC 30-2005) supplemented with 20% FBS. ATCC CCL-243 cells (lymphoblastic cells isolated from the pleural effusion of a patient with chronic myelogenous leukemia in terminal blast crises, abbreviated K562) were cultured in IMDM (ATCC 30-2005) supplemented with 10% FBS (Life Technologies, 16000-077). Stemgent BJ human fibroblasts were cultured in DMEM and F-12 (Life Technologies) supplemented with 10% FBS. All cultures were passaged using 0.05% trypsin supplemented with 0.02% EDTA or using 1 \times TrypLE Select (Life Technologies). For systems verification tests of capture efficiency, primary cells were obtained from splenocytes (AllCells, LLC PB003F) and peripheral blood mononuclear cells (AllCells, LLC PB003F).

De-identified fetal cortical tissue samples were collected from elective pregnancy termination specimens at San Francisco General Hospital. Tissue was collected with previous patient consent in strict observance of the legal and institutional ethical regulations. Protocols were approved by the Human Gamete, Embryo and Stem Cell Research Committee (institutional review board) at the University of California, San Francisco. Neocortical tissue sample spanning the thickness of the cortical wall was embedded in 3.5% low-melting-point agarose (Fisher) and sectioned using a Leica VT1200S vibrating blade microtome to 300- μm slices in artificial cerebrospinal fluid (ACSF) containing 125 mM NaCl, 2.5 mM KCl, 1 mM MgCl_2 , 1 mM CaCl_2 and 1.25 mM NaH_2PO_4 . The germinal region of the GW16 neocortex was microdissected using a microsurgical blade. The samples were centrifuged for 5 min at 300g, and residual ACSF was replaced with a prewarmed working solution of papain freshly diluted in Earl's balanced salt solution according to the manufacturer's instructions (Worthington Biochem. Corp.). The samples were incubated at 37°C for 20–30 min and centrifuged for 5 min at 300g. After removing the papain and DNaseI supernatant, tissue was resuspended in 1 ml of sterile Dulbecco's PBS (DPBS) containing 3% FBS (Sigma) and manually triturated by pipetting up and down approximately ten times. The suspension was passed through a 40- μm strainer cap (BD Falcon) to yield a uniform single-cell suspension. Cells collected from the primary GW21 cortex (ScienCell, cat. number 1520, lot number 9298) were thawed and either mixed directly with C_1 Cell Suspension Reagent for cell loading or cultured in a six-well plate precoated with poly-L-ornithine (Sigma) and laminin (Sigma) at 10 $\mu\text{g}/\text{ml}$. Complete neuronal medium (ScienCell, 1521) was replaced every other day for 19 d.

Cell loading, mRNA-seq library preparation and sequencing. Adherent cultures were dissociated using 0.05% trypsin supplemented with 0.02% EDTA or using

TrypLE Select (Life Technologies). After centrifugation and removal of the dissociation medium, cells were resuspended at a concentration of 150–500 cells/ μl . This cell suspension was mixed with C_1 Cell Suspension Reagent (Fluidigm, 634833) at the recommended ratio of 3:2 immediately before loading 5 μl of this final mix on the C_1 IFC along with 20 μl of freshly prepared staining buffer (2.5 μl ethidium homodimer-1 and 0.625 μl calcein AM from Life Technology's LIVE/DEAD Viability/Cytotoxicity Kit added to 1.25 ml C_1 Cell Wash Buffer) in their respective input wells. Images of captured cells were collected with a Leica DMI 4000B microscope in the brightfield, GFP and CY3 channels using Surveyor V7.0.0.9 MT software (Objective Imaging).

Single-cell RNA extraction and mRNA amplification were performed on the C_1 Single-Cell Auto Prep Integrated Fluidic Circuit (IFC) following the methods described in the protocol (PN 100-7168, <http://www.fluidigm.com/>). For experiments in which exogenous spike-in controls were used, the spikes were added to the lysis mix at a 20,000-fold dilution. The PCR thermal protocol was adapted from a recent publication that optimized template-switching chemistry for single-cell mRNA-seq³³ and is outlined in the C_1 Single-Cell Auto Prep System protocol. For the population control experiment, we used reagent formulations and workflows exactly as described in the SMARTer Ultra Low RNA Kit user manual (634833, 1 kit for 10 C_1 IFCs), except that the thermal protocol followed the recommendations outlined in the C_1 Single-Cell Auto Prep System user guide (PN 100-7168).

For the population control experiment, we sorted 100 K562 cells into 3.5 μl of Clontech Reaction Buffer containing exogenous spike-in controls using a BD FACSAria III. The 20,000-fold-diluted ERCC spike-in controls were further diluted (9:3,500) in Clontech Reaction Buffer such that an equal mass (rather than an equal concentration) of the spikes was included in the population control reaction. After the sort, cells were frozen at -80°C overnight before continuing the SMARTer Ultra Low RNA Kit protocol according to the manufacturer's recommendations.

The cDNA reaction products were quantified using the Quant-iT PicoGreen dsDNA (double-stranded DNA) Assay Kit (Life Technologies) and high-sensitivity DNA chips (Agilent) and were then diluted to a final concentration of 0.15–0.30 ng/ μl using C_1 Harvest Reagent. The diluted cDNA reaction products were then converted into mRNA-seq libraries using the Nextera XT DNA Sample Preparation Kit (Illumina, FC-131-1096 and FC-131-1002, 1 kit used for 4 C_1 IFCs and 384 samples) following the manufacturer's instructions with minor modifications. Specifically, reactions were run at one-quarter of the recommended volume, the fragmentation step was extended to 10 min, and the extension time during the PCR step was increased from 30 to 60 s. After the PCR step, samples were pooled, cleaned twice with 0.9 \times Agencourt AMPure XP SPRI beads (Beckman Coulter), eluted in Tris + EDTA buffer and quantified using a high-sensitivity DNA chip (Agilent). For high-coverage sequencing, libraries from a subset of captured cells from each source were pooled to reach a target of ten million aligned reads per cell.

Processing the mRNA sequencing data. An index for RNA-Seq by expectation maximization (RSEM) was generated on the basis of the hg19 RefSeq transcriptome downloaded from the UCSC Genome Browser database³⁴ (23,637 total genes). Read data were aligned directly to this index using RSEM/bowtie^{29,35}. FASTQ files from high-coverage sequencing data were downsampled to 11 sequencing depths (100; 500; 1,000; 5,000; 10,000; 50,000; 100,000; 150,000; 200,000; 250,000; and 300,000 reads) using a Python script to randomly select reads, and downsampled results were also aligned to the same index using RSEM/bowtie. Quantification of gene expression levels in TPM for all genes in all samples was performed using RSEM v1.2.4 (ref. 29). Genomic mappings were performed with TopHat v2.0.4 (ref. 36), and the resulting alignments were used to calculate genomic mapping percentages. Raw sequencing read data were aligned directly to the human rRNA sequences NR_003287.1 (28s), NR_003286.1 (18s) and NR_003285.2 (5.8S) using bowtie v2.0, and the percentage of reads aligned to rRNA was then calculated as reads aligned to these sequences divided by the total reads. Linear expression data were imported into the Fluidigm SINGuLAR Analysis Toolset 2.0 (the R scripts and user guide can be found at <http://www.fluidigm.com>) and converted into log-space. Transcripts with TPM values less than 1 were dropped from further analysis before log transformation. To identify outlier cells from each chip, we considered a set of genes detected in at least half of the samples,

and samples with median expression values below the 15th percentile for these genes were removed using the `identifyOutliers` function in the SINGULAR package. No additional normalization was performed between individual samples. Sequencing results obtained from capture sites with no detectable calcein AM staining that were not flagged as sequencing outliers were retained in the data set. Capture sites containing multiple live cells on the basis of calcein AM staining or brightfield microscopy were removed from further analysis. To assess technical variation during library preparation, we split cDNA from a single cell (GW21+3_1) into two samples, and two independent libraries were prepared with the Nextera XT DNA Sample Preparation Kit (Illumina). The correlation between \log_2 TPM expression values for technical replicates (0.993) was greater than that between any pair of distinct cells.

PCA and clustering. PCA was performed in the Fluidigm SINGULAR Analysis Toolset 2.0 R package, which calls the `princomp` R package (<http://stat.ethz.ch/R-manual/R-patched/library/stats/html/princomp.html>). The 500 top-ranked PCA genes were selected on the basis of the maximum absolute value of each gene loading score in the first three eigenvectors (PC1, PC2 and PC3). To compare sample scores between downsampling low-coverage data sets with high-coverage mRNA-seq data sets (Fig. 2 and Supplementary Fig. 9), the eigenvectors derived from the high-coverage data were applied to the low-coverage data using the `applyPCA` function in the SINGULAR package. Hierarchical clustering of the top 500 PCA genes across 301 cells was also performed in the Fluidigm SINGULAR package. Genes are clustered on the basis of Pearson correlation. Samples are clustered on the basis of a Euclidean distance matrix with complete linkage. Significance of the cluster assignment shown in Supplementary Figures 9 and 10 was tested using `Pvclust`³⁷, which employs a multiple bootstrap resampling algorithm to calculate the approximately unbiased (AU) probability values for cluster distinctions. We performed the clustering for 50,000 bootstraps.

Comparison of low- and high-coverage gene expression data. Pearson's correlation coefficients were calculated using the log-transformed TPM values for genes shared in both the low- and high-coverage data sets ($\text{TPM}_{\text{low}} > 1$ and $\text{TPM}_{\text{high}} > 1$) and also separately for all genes shown in Supplementary Figure 2. In addition, gene transcripts were binned, on the basis of the high-coverage data, into low-expression ($1 < \text{TPM}_{\text{high}} < 10$), medium-expression ($10 \leq \text{TPM}_{\text{high}} \leq 100$) and high-expression ($100 < \text{TPM}_{\text{high}}$) bins, and Pearson's correlation coefficients were again calculated for each of these subsets. We assessed the number of dropouts ($\text{TPM} < 1$) that were excluded from the correlation analysis by counting the number of genes that were detected only in the low-coverage data ($1 < \text{TPM}_{\text{low}}$ and $\text{TPM}_{\text{high}} \leq 1$) and the number of genes that were detected only in the high-coverage data ($1 < \text{TPM}_{\text{high}}$ and $\text{TPM}_{\text{low}} \leq 1$).

Validation using K562 cells and population mRNA-seq data including spikes. An additional validation data set was generated using K562 cells with exogenous spike-in controls (Life Technologies, 4456740) delivered in the lysis reagent at a 20,000-fold dilution as described above. A total of 46 captured single cells, one empty reaction line and one population sample (100 K562 cells sorted into a standard SMARTer Ultra Low RNA Kit reaction) were sequenced at both low- and high-coverage for this validation data set. The sequences for the 92 ERCC spike-in controls were added to our RSEM index, and RSEM v1.2.4 (ref. 29) was used to quantify gene expression levels in units of TPM. The average expression level, coefficient of variation and detection frequency (based on a limit of detection of $\text{TPM} > 1$) was calculated for each of the 92 spike-in controls across the 46 single-cell capture events and plotted against known inputs (copies per reaction) of each spike-in control (Fig. 1d,e). In addition, these cells were used to determine the correlation between aggregated single-cell and population data as a function of the number of single-cell data sets included in the ensemble. For the range of ensemble sizes shown along the horizontal axis in Figure 2a, we randomly selected ten ensembles, measured the Pearson's correlation of each ensemble with the population and then averaged the Pearson's correlation across the ten ensembles. These 46 average correlation values between various cell groupings and the overall population were then plotted as a function of the number of cells included in the ensembles (Fig. 2b).

Analysis of PCA genes and candidate biomarkers in neural cells. To examine the number of distinct gene clusters among the top 500 PCA genes explaining variation across neural cells, we performed consensus clustering using GENE-E (<http://www.broadinstitute.org/cancer/software/GENE-E/>). Heat maps were visually inspected to identify the optimal number of gene clusters. On the basis of these results, *k*-means clustering with three clusters was performed with a Euclidean distance matrix (2,000 iterations) and 20 resampling iterations. To identify candidate cell type-specific biomarkers, we examined the Pearson correlation between each gene with that of an idealized gene with binary expression in only one group of cells as determined by grouping relationships in hierarchical clustering.

Gene expression data for the top 500 PCA genes included in Figure 3f,g were obtained from BrainSpan¹¹ across all cortical samples for all probes from a post-conception week 15 (GW17), a post-conception week 16 (GW18) and two post-conception week 21 (GW23) samples. For genes containing multiple probes, the log-transformed gene expression values were averaged. For each gene, expression values across 211 cortical germinal zone samples (ventricular zone and subventricular zone regions) and 388 nongerminal zone samples (intermediate zone, subplate and cortical plate regions) were displayed on a heat map shown in Figure 3f using GENE-E, maintaining the order of genes in Figure 3b. To evaluate the distribution of genes in the red, yellow and green gene clusters, we performed a Wilcoxon signed-rank test comparing each gene between the averaged germinal zone and nongerminal zone samples. 8/500 genes were not represented by microarray probes in the BrainSpan¹¹ data set: *HEPN1*, *SNURF*, *ZNF286B*, *LOC100507246* (*SNHG16*), *MPC1*, *ATRAID*, *TECR* and *FRMD6-AS1*. The same approach was used to examine the expression of candidate cell type-specific biomarkers shown in Supplementary Figure 11, but samples from the marginal zone and subplate granular layer were also included in the analysis, and results across samples were further averaged for distinct laminae.

Immunohistochemistry and *in situ* hybridization. Timed-pregnant Swiss Webster mice were obtained from Simonsen Laboratories and maintained according to protocols approved by the UCSF Institutional Animal Care and Use Committee. Pregnant dams were deeply anesthetized with inhaled isoflurane and euthanized by cervical dislocation, and two litters were collected. Embryos were decapitated, and dissected brains were fixed in 4% paraformaldehyde overnight. A timed-pregnant ferret (Marshall BioResources) was maintained according to protocols approved by the UCSF Institutional Animal Care and Use Committee. The E35 pregnant dam was deeply anesthetized with ketamine before the administration of inhaled isoflurane. Ovariohysterectomy for fetus collection was performed for embryo collection. Embryos were perfused transcardially with cold PBS and 4% paraformaldehyde. Dissected brains were fixed in 4% paraformaldehyde overnight.

For immunohistochemistry and *in situ* hybridization, human fetal cortical samples were fixed overnight in 4% paraformaldehyde, cryoprotected in 30% sucrose and embedded in a 1:1 mixture of 30% sucrose and optimal cutting temperature compound (Thermo Scientific). Thin 20- μm cryosections were collected on superfrost slides (VWR) using a Leica CM3050S cryostat. For immunohistochemistry, heat-induced antigen retrieval was performed in 10 mM sodium citrate buffer, pH 6. For antibodies to CAMKV, NTM and SYNC, we did not perform antigen retrieval. Primary antibodies to ADRA2A (1:100, Thermo Scientific, PA1-048), CAMKV (1:100, Novus Biologicals, NBP1-68097), EGR1 (1:50, Cell Signaling, 41535), C-FOS (1:100, Santa Cruz, SC-8047), CTIP2 (1:500, Abcam, ab18465), NTM (1:100, R&D Systems, AF1235), phosphorylated vimentin (Ser82) (1:500, MBL International, D095-3), SATB2 (1:250, Santa Cruz, SC81376), SOX2 (1:200, Santa Cruz, SC17320) and SYNC, isoform 1 (1:100, a kind gift from K. Davies, University of Oxford) were diluted in blocking buffer containing 10% donkey serum, 0.5% Triton X-100 and 0.2% gelatin. Binding was revealed using an appropriate Alexa Fluor 488 (A21206), Alexa Fluor 546 (A11056) or Alexa Fluor 647 (A31471) fluorophore-conjugated secondary antibody (Life Technologies). Cell nuclei were counterstained using 4',6-diamidino-2-phenylindole (Life Technologies). Images were collected using a Leica TCS SP5 X confocal microscope and processed using ImageJ or Imaris (Bitplane).

Probes complementary to the target human mRNA used for RNA *in situ* hybridization were generated specifically for this study, except for *EMX2*,

which was generated against the mouse sequence and generously provided by A. Simeone (Institute of Genetics and Biophysics, Adriano Buzzati-Traverso). To generate RNA *in situ* probes, we extracted total RNA from primary human cortical samples aged GW14–GW21 using the RNeasy RNA extraction kit (Qiagen) and reverse transcribed it with the Superscript III First Strand Synthesis System with random hexamers (Life Technologies). Primers specific to the target genes of interest were designed using Primer3 and amplified by PCR using Phusion proofreading DNA polymerase (Thermo Scientific). Specific genes were amplified using the following primers: *ANXA2*: forward primer, CCA GGA GCT GCA GGA AAT TA, reverse primer, TGT TAG CTG GAA GCA TGG TG (it should be noted that the target *ANXA2* mRNA sequence is indistinguishable from a related retrotransposed pseudogene, *ANXAP2*, and our probe would not distinguish between transcripts from these loci); *C1orf61*: forward primer, TCC AAG AAG AAG CAG CCT CA, reverse primer, CAG GTA CAG TGG GCT TCC TG; *CKS2*: forward primer, GCG CTC TCG TTT CAT TTT CT, reverse primer, GCA CTT AAG AGA AAA ACT GAC TGG; *CLU*: forward primer, CGG AGG CCT CAC TTC TTC TT, reverse primer, GTA TTC CTG CAG CGC TTT CT; *DDAH1*: forward primer, CCC CTA AGC CTC CCG AAG, reverse primer, TAG CGG TGG TCA CTC ATC TG; *EGR1*: forward primer, CTG CAC GCT TCT CAG TGT TC, reverse primer, CAT GTC CCT CAC AAT TGC AC; *FOS*: forward primer, AGC AGT GAC CGT GCT CCT AC, reverse primer, CAG GAA CCC TCT AGG GAA GA; *GRIA2*: forward primer, TGT TTT ATT GCA AGT GGT CCA A, reverse primer, ATC CAC ACT GGG CAT ATT AAA; *HES1*: forward primer, TTT AGC ACT CCT TCC CGT TG, reverse primer, AAA CAC CTT AGC CGC CTC TC; *HMGB2*: forward primer, GCC ATT TTT CAA ACC CTC TTC, reverse primer, CAC CTT TGG GAG GAA CGT AA; *NNAT*: forward primer, TTT CTC GAC CAC CCA CCT AC, reverse primer, AGG AGC ACC TGA TGA TAC GG; *PDZRN3*: forward primer, AGC AAC GAG TCT TTC ATT TCG, reverse primer, GCT CTC CGC TCT TTG CTT T; *PON2*: forward primer, CCG AAG GTA TCT GGG GAA AT, reverse primer, TTG ATC CCA TTT GCT GAA TC; *RTNI*: forward primer, CCC CTC CCT CCA GTA CCA TA, reverse primer, TGA ATC CAT TAG GAA CTA CAG AGA AA; *SCG5*: forward primer, GGT ACC CAG ACC CTC CAA AT, reverse primer, CCA AGG GCT GGA TGA ACT AC; *SPARC*: forward primer, CTT CAG ACT GCC CGG AGA, reverse primer, CAG GCG CTT CTC ATT CTC AT; *SRGAP3*: forward primer, CCG AGA AGA TGT TCC CCA AC, reverse primer, CGC AGT TAC TAT GGG CCT TT; *STMN2*: forward primer, AAT GGA TCA TGC GAT ATC AGG, reverse primer, GCC AAA GCA CAT TTG TAG CA; *TAGLN3*: forward primer, GGG CTT GAT TGA CAC AGG AG, reverse primer, GAA CTG GGA GAT TTG CTC CA; *TFAP2C*: forward primer, GAC CCC TAC TCG CAT CTG G, reverse primer, AGA GTC ACA TGA GCG GCT TT; *TTYH1*: forward primer, GGC AAC AGT GAG ACC AGT GA, reverse primer, AAC TGA GGC ACA GCT TCT CG. PCR products of predicted band size were gel extracted and A-tailed using GoTaq DNA Polymerase (Promega) and ligated into the pGEM T-Easy Vector System (Promega). Ligation products were transfected into One Shot TOP10 Chemically Competent *Escherichia coli* (Life Technologies). Cloned probe sequences were confirmed by sequencing. Digoxigenin (DIG)-labeled RNA probes for *in situ* hybridization were generated by linearizing the pGEM T-Easy Vector and *in vitro* transcribing the probe using T7 or SP6 RNA Polymerase (Roche) in the presence of DIG-RNA Labeling Mix (Roche). *In situ* hybridization was performed blinded to

the sense or antisense status for each probe, and sense control probes gave no signal (data not shown). The *in situ* hybridization protocol has been described before³⁸. For subsequent immunolabeling, slides were subjected to antigen retrieval as described above. Images were collected with a Leica DMI 4000B microscope using a Leica DFC295 camera.

Organotypic slice cultures. Human fetal cortical slices were collected as described above. Slices were transferred into slice culture inserts (Millicell) in six-well culture plates (Corning) and cultured in culture medium containing 66% BME, 25% Hank's balanced salt solution, 5% FBS, 1% N-2, 1% penicillin and streptomycin and glutamine (Life Technologies). Slices were cultured in a 37 °C incubator at 5% CO₂, 8% O₂ for 1 d. To induce Notch signaling, the culture medium was replaced completely with Ca²⁺-free ACSF containing 126 mM NaCl, 3 mM KCl, 1.2 mM NaH₂PO₄, 26 mM NaHCO₃, 2 mM MgCl₂, 1 mM EDTA and 10 mM D-glucose. Control slices were incubated in parallel with ACSF containing 126 mM NaCl, 3 mM KCl, 1.2 mM NaH₂PO₄, 26 mM NaHCO₃, 1.3 mM MgCl₂, 2.4 mM CaCl₂ and 10 mM D-glucose. All slice cultures were placed in a 37 °C incubator at 5% CO₂, 8% O₂ for the duration of the treatment. After a 10-min, 20-min or 30- to 40-min incubation, the slices were either frozen on dry ice and stored at –80 °C in RNase-free tubes or fixed with 4% paraformaldehyde for 20 min at 4 °C and processed for cryosectioning as described above.

Quantitative RT-PCR. RNA extraction and cDNA synthesis were performed as described above, and quantitative RT-PCR was performed using the QuantiTect SYBR Green PCR Mix (Qiagen) in a Roche LightCycler 480 II. The following primer pairs were used in this study to detect specific mRNAs, blinded to the treatment status of each sample: *GAPDH*: forward primer, GAG TCA ACG GAT TTG GTC GT, reverse primer, TTG ATT TTG GAG GGA TCT CG; *ACTB*: forward primer, GGA CTT CGA GCA AGA GAT GG, reverse primer, AGC ACT GTT GGC GTA CAG; *HPGK*: forward primer, CTG TGG GGG TAT TTG AAT GG, reverse primer, CTT CCA GGA GCT CCA AAC TG; *TFAP2C*: forward primer, TCA GTC CCT GGA AGA TTG TCG, reverse primer, CCA GTA ACG AGG CAT TTA AGC A; *EGR1*: forward primer, ACC CCT CTG TCT ACT ATT AAG GC, reverse primer, TGG GAC TGG TAG CTG GTA TTG. Quantification and comparisons of gene expression levels were performed using the –ΔΔC_t method, and statistical analyses of differences between control and EDTA-treated samples were performed using paired two-tailed Student's *t*-test.

33. Fan, J.B. *et al.* Highly parallel genome-wide expression analysis of single mammalian cells. *PLoS ONE* **7**, e30794 (2012).
34. Fujita, P.A. *et al.* The UCSC Genome Browser database: update 2011. *Nucleic Acids Res.* **39**, D876–D882 (2011).
35. Langmead, B., Trapnell, C., Pop, M. & Salzberg, S.L. Ultrafast and memory-efficient alignment of short DNA sequences to the human genome. *Genome Biol.* **10**, R25 (2009).
36. Trapnell, C., Pachter, L. & Salzberg, S.L. TopHat: discovering splice junctions with RNA-Seq. *Bioinformatics* **25**, 1105–1111 (2009).
37. Suzuki, R. & Shimodaira, H. Pvcust: an R package for assessing the uncertainty in hierarchical clustering. *Bioinformatics* **22**, 1540–1542 (2006).
38. Wallace, V.A. & Raff, M.C. A role for Sonic hedgehog in axon-to-astrocyte signalling in the rodent optic nerve. *Development* **126**, 2901–2909 (1999).